Vibrations:
a mode of thinking

Simon Lacoste-Julien
Mathieu Plamondon

Lab Report
Department of Physics
McGill University

March 11, 2002

Abstract

A square aluminum plate with clamped edges is driven with sound waves and its lateral deformations are detected with a photodiode. Natural frequencies and mode shapes are evaluated and compared to theoretical predictions for a thin plate having these boundary conditions. Our results validate the predicted spectrum and showed the presence of degenerate modes. Further analysis of the Q-factor and the hysteresis increase understanding of plates' behaviour.

1 Introduction

Anybody curious about natural phenomena can witness oscillations almost anywhere, from the realm of atoms to pulsars. As expected, a great part of physics has been dedicated to the study of this common behaviour. For example, understanding this property can be a precious skill in order to explain the acoustics of a guitar, populations' cycles in biology, emissions of radiations from an antenna, fluctuations in stock market, etc. Often, we search the response of a system to stimuli. This becomes crucial in industry where structures like planes' wings or bridges must resist to vibrations. Motivated by these applications, our experiment treats with a more tractable case: lateral deformations of a thin square aluminum plate with clamped edges.

The purpose of this experiment is to study experimentally the properties of vibration of a aluminum plate with clamped edges and driven by sound waves, and compare it with the theory.

What information can be extracted from this simple object? The first observation is dictated by the existence of a spectrum: the plate responds more to specific discrete frequencies when driven by a sound wave. Large amplitudes are observed at resonance and an attempt is made in order to have there a picture of the surface. Mode shapes and natural frequencies will then be compared to the theory which predicts them simultaneously under certain conditions. But nothing stays limpid as soon as we take a closer look. Many measurements exhibit actually a superposition of degenerate modes as in quantum mechanics. After, the effects of friction are taken into account and the evaluation of the Q-factor gives an idea of their importance. Pushing further our investigations, we remove the assumption of the linearity in the response of the material by overdriving the plate. A complicated behaviour called hysteresis governs now the dynamics.

2 Theory

2.1 Vibrating modes

Throughout this experiment, we are interested about the lateral displacements z(x,y) of a thin plate. Its bending rigidity due to its thickness and the elasticity of the material distinguish it from a membrane. A careful consideration of stresses and strains involved (see [6]) leads to this fundamental equation of motion:

$$D\nabla^4 z(x,y,t) + \rho\frac{\partial^2}{\partial t^2} z(x,y,t) = 0 \tag{1}$$

where ρ is the mass density per unit area of the plate and D, called the flexural rigidity, is defined as:

$$D \equiv \frac{Eh^3}{12(1-\nu^2)} \tag{2}$$

where E, h and ν are the Young's modulus, the thickness of the plate and the Poisson's ratio respectively. The simplicity of this result suggests that many assumptions were made during the derivation:

- the plate has a non-varying thickness
- the material of the plate has simple properties: homogeneity, linear elasticity and isotropy
- we neglect rotary inertia; shear deformations are small relative to the thickness of the plate deformations
- there is no in-plane load in the plate
- the thickness to lateral plate dimension ratio is small

The 4^{th} order of equation (1) imposes the determination of eight boundary conditions:

$$z(\pm\frac{a}{2}, y) = z(x, \pm\frac{a}{2}) = \left[\frac{\partial z(x,y)}{\partial x}\right]_{x=\pm\frac{a}{2}} = \left[\frac{\partial z(x,y)}{\partial y}\right]_{y=\pm\frac{a}{2}} = 0 \tag{3}$$

This corresponds to the fact that our square plate of length a has its four edges clamped. For free vibrations at frequency w, we could expect a solution of the form:

$$z(x, y, t) \propto z(x, y)sin(\omega t + \phi) \tag{4}$$

Substituting in (1), we obtain

$$(\nabla^4 z - \frac{\rho\omega^2}{D})z(x, y) = (\nabla^2 - k^2)(\nabla^2 + k^2)z(x, y) = 0 \tag{5}$$

where $k^2 = \sqrt{\frac{\rho\omega^2}{D}}$. It is shown in [4] that equation (1) yields two eigenvalue equations of second order for k. As with the usual Sturm-Liouville formalism, the trivial boundary conditions given allow a complete countable infinite family of orthogonal solutions z_{ij} depending on two integer parameters i and j. Each of those $z_{ij}(x, y)$ is what we called **mode of vibration**, and their orthogonality arises from our clamped boundary conditions, as demonstrated in [1]. For our clamped boundary conditions, it appears that the $z_{ij}(x, y)$'s are product of sine and cosines with modulating hyperbolic functions. Graphs of those specific solutions for the first modes were provided to us by Mark Orchard-Webb (see [7]), and are given in annex B. Also, the index i can be seen to represent the number + 1 of node lines parallel to the y-axis. And similarly for j with the y-axis replaced by the x-axis.

Using the principle of superposition, we can obtain the general solution:

$$Z(x, y, t) = \sum_{i=1}^{\infty}\sum_{j=1}^{\infty} A_{ij} z_{ij}(x, y)sin(\omega_{ij} t + \phi_{ij}) \tag{6}$$

where the phases ϕ_{ij} and the constants A_{ij} are determined by the initial and boundary conditions. From that, we deduce a qualitative property for the modular distribution: the presence of symmetric and antisymmetric mode shapes relative to each axis. Now the orthogonality of this basis implies that if we drive the system at one of the eigenfrequencies ω_{ij}, all the terms vanish except those with the same eigenfrequencies (degeneracy happens when $i \neq j$). We can thus excite specific modes of the system. An analogy can be made with a measurement in quantum mechanics which projects the system into one of its eigenstates. Finally, the eigenvalues k^2 give an expression for the natural frequencies in terms of i and j:

$$f_{ij} = \frac{\omega_{ij}}{2\pi} = \frac{{\lambda_{ij}}^2}{2\pi a^2}\sqrt{\frac{D}{\rho}} \tag{7}$$

where ${\lambda_{ij}}^2$'s are dimensionless parameters, function of the mode, and which are given in [6].

2.2 Q-factor and decay

The quality factor Q characterizes the degree of damping of an oscillating system and can be defined as the ratio of the energy stored in the oscillator to energy lost per radian of oscillation. Hence, from this definition, it can be deduced that lightly damped oscillators have large Q's in comparison to those heavily damped. Toward this notion, we consider a small area dA of the plate and approximate its equation of motion to a forced damped harmonic oscillator:

$$F = (\rho\ddot{z})dA = F_{spring} + F_{damping} + F_{driving} = (-kz - b\dot{z} + F_0 \cos\omega t)dA \tag{8}$$

where F_0 is the amplitude per unit area of the driving force at angular frequency ω due to the speaker. Similarly, k represents locally the spring constant related to the rigidity of the material and b, a damping factor. We obtain

$$\ddot{z} + \gamma\dot{z} + {\omega_0}^2 z = \frac{F_0}{\rho}\cos\omega t \tag{9}$$

in which $\gamma = \frac{b}{\rho}$ and ${\omega_0}^2 = \frac{k}{\rho}$. The γ factor is directly observed by an analysis of the transient behavior. Without forcing, we remark a decrease in the frequency

$$z(t) = A(t)cos\left[\omega_1 t + \phi\right] = Ae^{-\frac{\gamma t}{2}}cos\left[\omega_1 t + \phi\right] \tag{10}$$

since $\omega_1 = \sqrt{{\omega_0}^2 - \frac{\gamma^2}{4}}$. Also, notice that the amplitude is exponentially decaying. The average energy $\langle E(\omega)\rangle$ being proportional to $A(t)^2$, it can be shown (see [3]) for small damping ($\gamma \ll \omega_1$) that the average energy follows an exponential decay

$$E(t) = E_0 e^{-\gamma t} \tag{11}$$

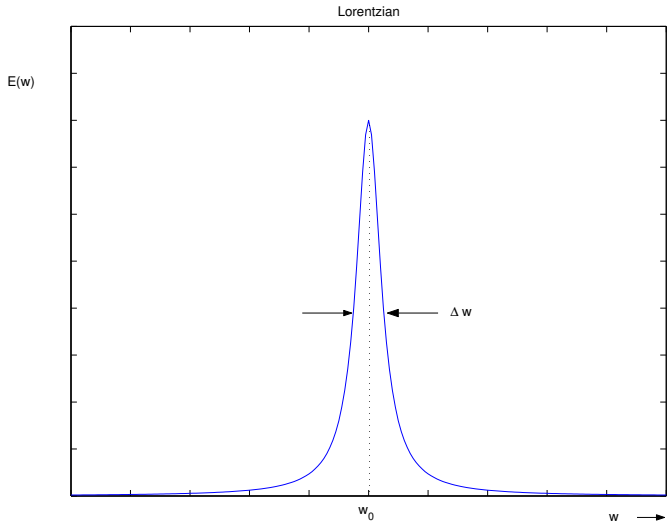

Figure 1: **Lorentzian and FWHM** $\Delta\omega$ ω_0 is the resonant frequency.

and that Q is given by the simple formula

$$Q = \frac{E}{\triangle E \text{ per radian}} = \frac{\omega_0}{\gamma} \tag{12}$$

In a second step, we come back to equation (9) and find this time the steady-state behavior for the lateral displacement. The solution takes the form $z = A\cos(\omega t + \phi)$ with amplitudes A and phase ϕ given by

$$A = \frac{F_0}{\rho\left[(\omega_0{}^2 - \omega^2)^2 - (\gamma\omega)^2\right]^{\frac{1}{2}}} \tag{13}$$

$$\phi = \arctan\left[\frac{\gamma\omega}{\omega^2 - \omega_0{}^2}\right] \tag{14}$$

An exact expression for $\langle E(\omega)\rangle$ can be derived (see [3]). Assuming again light damping, it exhibits a Lorentzian shape as in figure 1 with maximum amplitude when $\omega = \omega_0$, at resonance. Sketched on the picture, the bandwidth $\triangle\omega$ is calculated at half this maximum and actually equals γ. We use equation (12) and arrive to this relationship:

$$\langle E(\omega)\rangle \propto \frac{1}{\left(\frac{\omega}{\omega_0} - 1\right)^2 + \frac{1}{4Q^2}} \tag{15}$$

The analysis of these resonance peaks provides an alternative way of evaluating the Q of the system. Finally, the fact that at resonance we observe a phase shift in equation (14) and on picture 2 facilitates the determination of the natural frequencies during the experiment (see section 3.3.2).

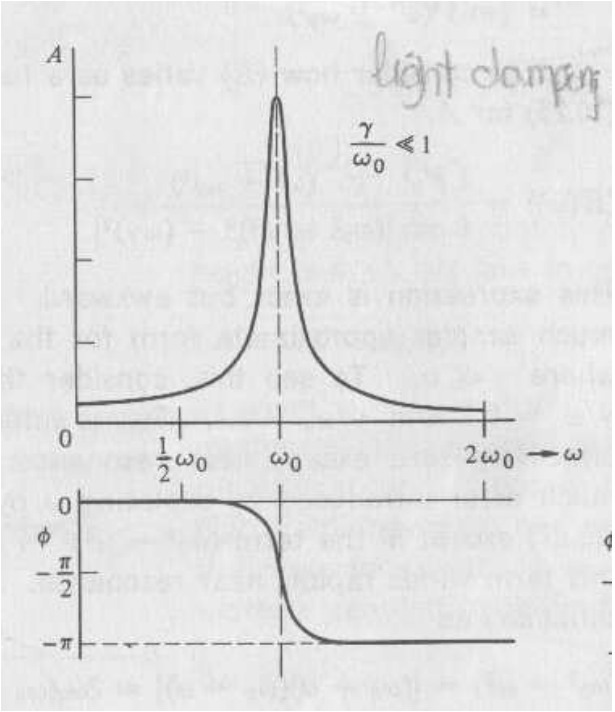

Figure 2: **Lorentzian and phase shift.** This picture was taken in [3], p. 425. ϕ represents the phase between the driving force and the response of the oscillating system.

2.3 Lock-In system

In our lab, the Lock-In component achieved the same task that we describe in this section. The mathematical problem consists of extracting information about the the amplitude A and phase ϕ from a signal $V_s(t) = A\sin(\omega t + \phi)$ of known frequency. A reference square wave V_{ref0} in phase with V_s and having the same frequency ω is generated. Superposing these functions, we calculate the mean value over a period T of this resulting signal and find:

$$\langle V_0 \rangle = \langle V_s(t) V_{ref0}(t) \rangle = \frac{1}{T} \int_0^T V_s(t) V_{ref0}(t) dt \propto A\cos\phi \tag{16}$$

The same procedure can be completed using another reference signal V_{ref90} with the same shape but now out of phase with V_s. A similar integration leads to $\langle V_{90} \rangle = \langle V_s(t) V_{ref90}(t) \rangle \propto A\sin\phi$ with the same proportionality constant. Combining these relations, we obtain expressions for A and ϕ.

$$A \propto \left[\langle V_0 \rangle^2 + \langle V_{90} \rangle^2 \right]^{\frac{1}{2}} \tag{17}$$

$$tan(\phi) = -\frac{\langle V_{90} \rangle}{\langle V_0 \rangle} \tag{18}$$

Note that these results are sufficient for our purposes since only the general shape of the amplitude is needed rather than its precise value in this experiment.

2.4 Non-linear oscillations

A brief discussion here shows the main results that are derived in [5] and [2]. When anharmonic terms are added in the equation of motion, a perturbation expansion reveals an amplitude dependence of the eigenfrequencies. The non-linearity removes the symmetry of the resonance curves (see parts a) and b) of figure 3). Near resonance, the amplitude of oscillation can possess three solutions contained in a cubic equation.

Physically, we remark a peculiar behaviour called hysteresis: two amplitudes of oscillation are possible for the same driving frequency and depend on the path used. If we gradually increase the frequency, the amplitude increases along ABC (see figure 3, part c) and falls discontinuously to E. On the other hand, a decrease in frequencies will exhibit an abrupt gain occurring at the lower value D.

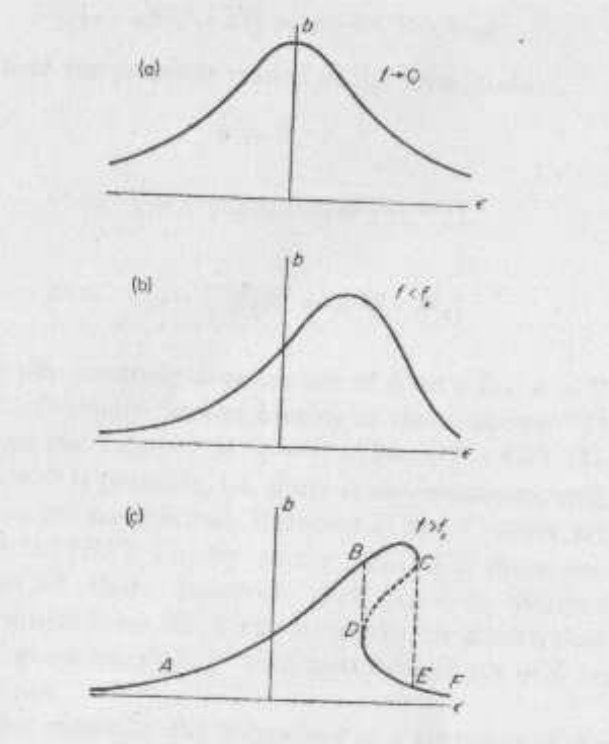

Figure 3: **Non-linearity effects in the amplitude shape.** Note the hysteresis of amplitude in part c) of the picture. This picture was taken on p. 89 of [5]

3 Experimental Procedure

3.1 Overview

Considerable amount of time in this laboratory was spent doing experimental manipulations. The experimental setup was not overly complex, but needed some time to become acquainted with, and needed many fine tuning. Section 3.2 will describe in details this intricate setup.

We can organize the experimental manipulations for this lab in three parts: the preparation (section 3.3), the main experiment (section 3.4) and finally some complementary measures (section 3.5). During the preparation, we first assembled the setup which consisted mainly of an **audio system** which could excite the modes of vibration of an aluminum plate clamped in a metallic frame; a **mechanical system** which held a sensor just above the plate to detect its vibrations and which could be controlled remotely (by hand or with a computer); and an **analysis and control system** which consisted of an oscilloscope and a computer, connected to the other components through a Lab Master interface. After this assembly, the sensor was calibrated (see section 3.3.1) and the frequencies of resonance of the vibrating plate were found (roughly) using an oscilloscope to analyze the sensor output.

For the main experiment, we first did a complete mapping of the amplitude of vibration in function of the position on the plate, for different frequency ranges, using a software which could control the mechanical arm and the frequency of our audio system (see section 3.4.1). We then studied the damping behaviour of the vibration of the plate by measuring the amplitude of oscillation in function of time, at one point on the plate, just after turning off the audio system, using the computer and the Lab master.

Finally, as complementary measures, we drove the plate in the non-linear region using a higher volume, and measured the amplitude of vibration in function of frequency for different *paths* in the frequency space. This permitted us to study hysteresis. Also, we tried to break the degeneracy of the 1-2 mode by changing the orientation of the speaker with respect to the plate.

3.2 Setup and Apparatus

A block diagram describing the setup is shown in figure 4. The numbers written in parenthesis in the present section make reference to the corresponding parts in the block diagram. A picture of the mechanical region of interest for this experiment is shown in figure 5.

3.2.1 Drum assembly

A thin square aluminum plate (1) (15 cm of side) was suspended directly above a loudspeaker (2) which served as the time varying driving force for the vibrating plate. The plate was held solidly with clamped boundary conditions, parallel with the table, in a metallic frame. A mechanical arm held a sensor (3) (a

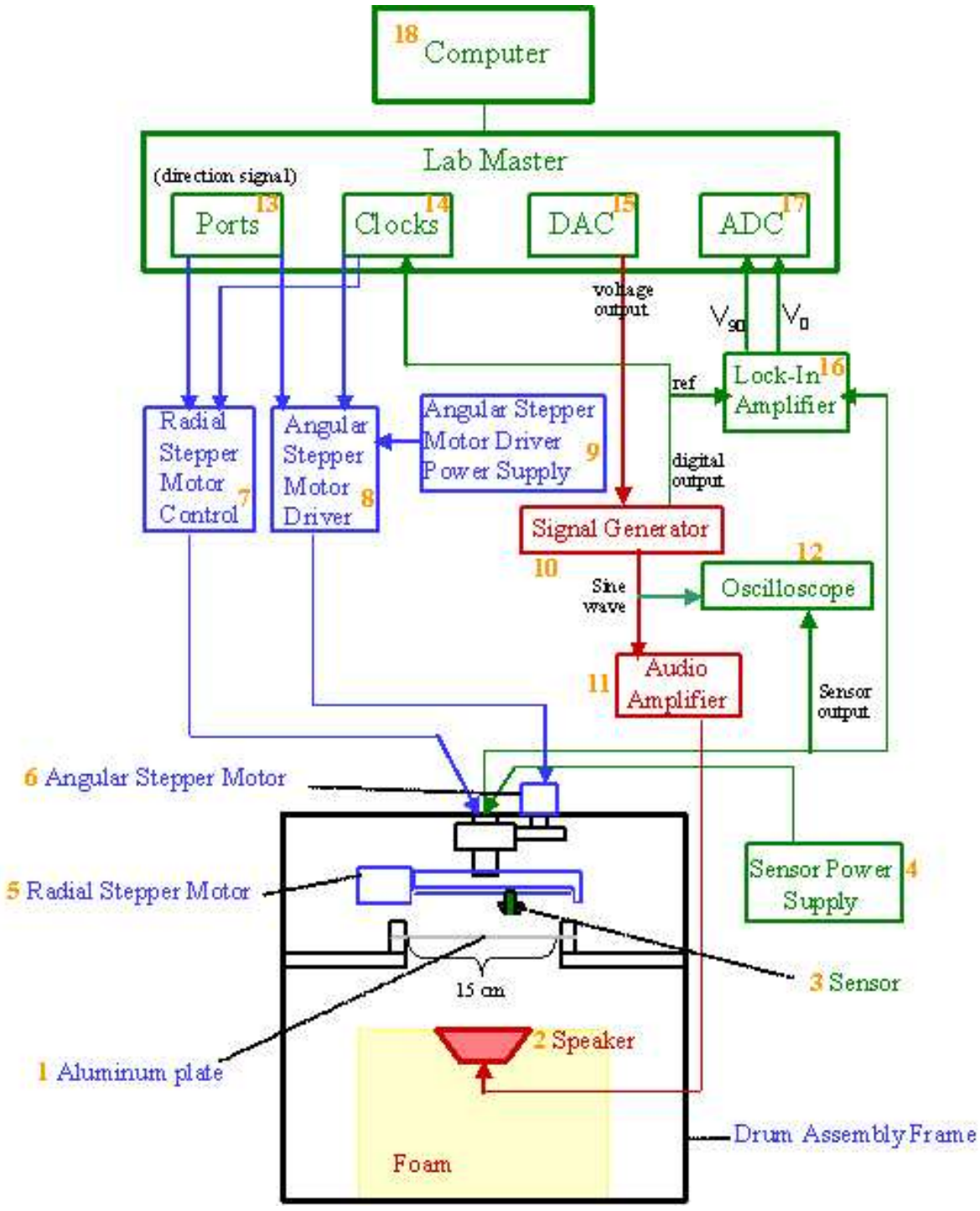

Figure 4: **Block diagram of experimental setup.** The mechanical system is shown in blue, the audio system is red and the control and analysis system is green.

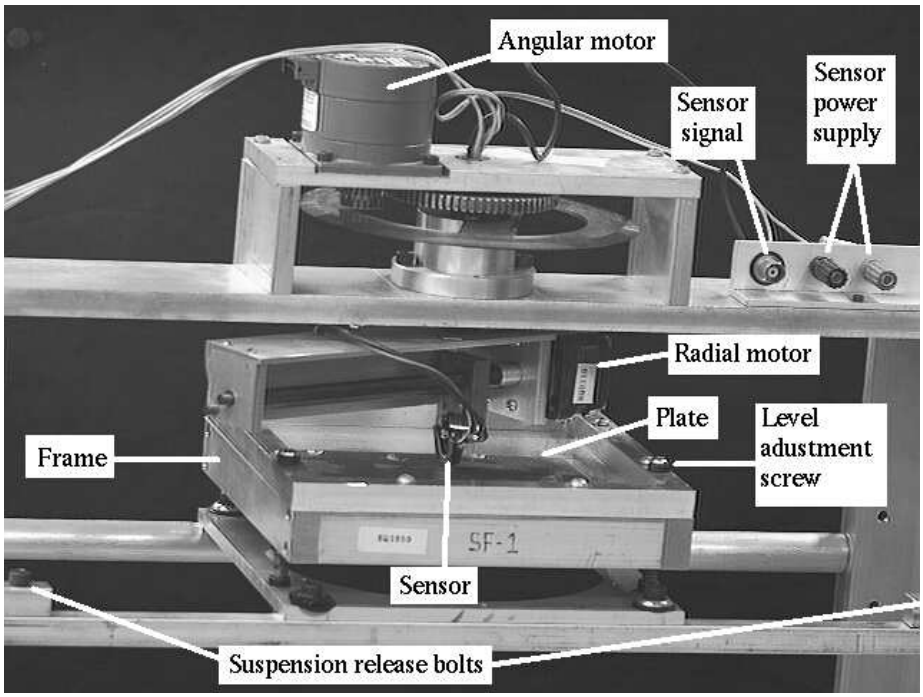

Figure 5: **Picture of mechanical region of interest.** This picture, representing the region around the vibrating plate, was taken from [7].

component consisting of an infra-red LED and a photo transistor in one package) at a fixed distance above the plate. A picture of this part, taken from [7], is shown in figure 5. The sensor was powered by a DC power supply (4) which was set at 24 Volts during the whole experiment (see the section 3.3.1 about calibration for more information about this). The level of the plate could be arranged with the level adjustment screws (see figure 5).

3.2.2 Motor system

Two stepper motors could control the movement of the sensor above the plate, one in the radial direction (5), and one in the angular direction (6), the axis of rotation being directly above the center of the plate. Each motor was steered by a driver ((7) and (8) for the radial and angular motor respectively) which could be either controlled manually, or remotely by the computer using the Lab Master. The angular motor had its own power supply (9), whereas the radial motor used the sensor power supply (4).

3.2.3 Audio system

A Wavetek signal generator (10) sent a sine wave to a conventional audio amplifier (11) which was in turn connected to a 5" loudspeaker (2), located just under the aluminum plate. The speaker was put on a foam box in order to attenuate its vibrations and to obtain a stable sound direction. The output of the signal generator was also feeded into the channel 1 of a Tektronix oscilloscope (13), in order to be compared with the signal from the sensor output, connected to the channel 2.

3.2.4 Lock-in amplifier

As described in the theory in section 2.3, a Lock-In system can be used to extract phase and amplitude information from a signal. The reference frequency was received from a digital output channel from the signal generator (10). The signal to analyze was given from the sensor output. The Lock-In amplified this latter signal and outputted the $< V_0 >$ and $< V_{90} >$ DC voltages which permitted us to compute the phase and the amplitude of vibration of the plate according to equations (17) and (18).

3.2.5 Computer, Lab Master and Softwares

We made heavy use of the computer in this experiment. The Lab Master permitted us to convert digital to analog signal and vice versa, in a format analyzable for the computer. The ports (13) in the Lab Master were used to send a continuous voltage to the motor control drivers which would determine their direction. The clocks (14) were used to send digital pulses to the motor drivers to make them run by steps. In addition, the digital output of the signal generator (10) was also connected to a clock, so that we could measure the frequency of our

driving force. A DAC (digital to analog converter) (15) was used to send a voltage to the signal generator in order to control, with the computer, the frequency of the sine wave produced. Finally, the output of the Lock-In amplifier (16) was transformed into a digital signal with the ADC channels (17) so that we could record the phase and amplitude information with the computer (18).

3.2.6 Computer and Softwares

Here is a list of the softwares that we used exclusively for this experiment. These were programmed in C by Mark Orchard-Webb (see [7] for the documentation). Each one will be described more in details with their use in their relevant sections.

- `motor` Used to control the motor.
- `freq_con` Used to control the frequency and study the output signal of the sensor.
- `drumscan` Used to scan the whole plate to find the amplitude of vibration in function of position.
- `makegrid` and `cart2rad` Used to build a grid of the plate in a format understandable by `drumscan`.
- `drumsamp` Used to study the decay of the oscillation.
- `drumscan_process` Used to analyze the output of `drumscan`.

3.3 Preparation

3.3.1 Calibration

The first thing we did was to find the output DC voltage of the sensor in function of its distance with the reflective surface. It was done with a vernier having a reflective surface glued on it; and the voltage was measured using a digital voltmeter[1]. The plot we found is shown in annex A, figure 18. Even if we can see on this graph that the sensor was saturated (according to the specifications for a TRW sensor, the curve should be smooth, not cut-off like ours), we decided to keep this calibration (with the power source for the sensor operated at 24 V) in order to have the maximum sensibility in the linear region. The slope of 21 V/mm means that we could measure oscillation of at most 8 V (to be safe), i.e. of about 0.3 mm, without getting out of the linear region. Later, it was checked on the oscilloscope that indeed the oscillations of the plate yielded a maximum variation of the voltage output of the sensor of the order of 1 or 2 Volt (so oscillations of about 0.1 mm maximum) (this was for non-linear oscillations of the plate). We have then positioned the plate at a distance of about 2 mm from

[1] We could witness the sensibility of the sensor during this part: putting scissors on the table where the vernier stood gave rise to variation of about 0.03 V!

the sensor (corresponding to a DC voltage of about 12 V), in order to be in the middle of the linear region, using the level adjustment screws. We then tried to make sure the distance between the plate and the sensor was kept constant as we move the sensor around the plate, by fiddling with the 4 adjustment screws. But we didn't succeed to reduce the variations under about 4 volts, because of the great sensibility of the sensor. Since only variation of voltage *at a point* would be measured, this didn't really matter. But it could mean that the plate wasn't totally parallel with the sensor surface, and this increases the error we make on the amplitude of oscillation we measure.

The other part of the preparation was to calibrate the motors. By controlling them with the program `motor` which could make them move by a specific number of steps given as argument, we could measure that the angular motor did a whole turn in 720 steps (hence 0.5 degrees per step) and that the radial motor made the sensor to travel for 55 ± 1 mm in 6000 steps, or $9.1 \pm 0.2 \mu m$ per step.

3.3.2 Finding resonant frequencies

Using an oscilloscope in X-Y mode, we could compare the amplitude and phase of oscillation of vibration of the plate vs. the signal sent to the speaker. As explained in the section 2.2 of the theory, there should be a 180° shift of the phase between the oscillating medium and the driving medium when passing the resonant frequency. On the screen of the oscilloscope in X-Y mode, we could observe a diagonal line transforming into an ellipse when we were approaching a resonant frequency. So by sweeping through frequencies between 50 Hz and 800 Hz and watching for ellipses on the oscilloscope, we could find roughly the first 6 resonant frequencies of the plate.

3.4 Main Experiment

3.4.1 Mapping Mode

After having identified roughly the resonant frequencies, we could start to study the amplitude of the vibration of the plate in function of position, close to these frequencies, using the scanning program.

By using the program `freq_con`, we could control (interactively) the frequency of the signal generator by integer steps (which corresponded roughly to 0.06 Hz per step for the 200 Hz scale of the generator) with the DAC output of the Lab Master (as shown in the block diagram in figure 4). The program also displayed in real time the phase and amplitude[2] information about the sensor signal, as computed from the V_0 and V_{90} outputs from the Lock-In amplifier with equations (17) and (18), connected to ADC channels in the Lab Master. The frequency of the signal generator was measured using its digital output connected to the Lab Master, and also displayed on screen. The ADC channels

[2]Of course, in the remaining of this lab, when we say that we measure the amplitude of oscillation, we mean simply that we are measuring something *proportional* to the amplitude. To measure its precise value, we would need a couple of proportionality constants which are not important in this qualitative laboratory...

of the Lab Master could accept only input voltages between -10 V and 10 V (and measured them with a precision of 5 mV). The Lock-In amplifier had a gain knob which permitted us to adjust its output voltage to be in this range.

So first, we tried to find the position on the plate of the maximum amplitude of oscillation at resonance using the `freq_con` program and the oscilloscope. Then, we lowered the level of the audio amplifier until we felt that if we would lower it more, we would obtain only noise signal and not a clean oscillation behavior (this was checked with the oscilloscope in X-Y mode). Finally we adjusted the gain of the Lock-In amplifier so that the maximum amplitude was about 5 V. This was done in order to be sure that we wouldn't saturate the ADC channel while scanning the whole plate, but that we would minimize the discreteness error by having a sufficiently high signal. Also, the reason why we tried to use very low volume of the audio amplifier for the mode mapping was to keep the oscillating system as much as possible in the linear region. On the other hand, we had to keep the volume high enough not to measure only noise. We needed a compromise between the two and this was done by fiddling around. Also, we noticed that the apparatus was very sensitive to outside disturbance (as voice, impacts, etc.). We have thus ran our mapping of the modes during the night (especially since there was construction being done very close by during the day!).

After having done those settings, we could use the `drumscan` program which did the plate scanning automatically. This program made the sensor follow a predefined grid above the plate, sweeping through a fixed frequency range at each point of the grid and recording the average and standard deviation from the mean of Lock-In signals at each frequency of driving, and outputted these to standard output (which could be redirected to a file for further analysis with the `drum_scan` program). It controlled the mechanical arm using the ports and clocks of the Lab Master (as already mentioned in section 3.2.5), with the calibration of the motors (see 3.3.1) given as a configuration file. The grid datafile was built using the `makegrid` and `cart2rad` programs which yielded an heuristically optimized path that the arm should follow (in polar angles) to cover the whole grid. The frequency range was chosen so that we were sure that the resonant frequency would be inside it (we have observed shifts of resonant frequency of about 5 Hz for different runs). A typical run of the program was with 2048 measures per frequency, a range of about 100 integer steps of frequency, and a 13x13 grid covering a region of 14 cm x 14 cm of the plate; and lasted around 3 hours. Using a batch file, we could program several runs during the night, for the same frequency region (since we couldn't hardly calibrate the gain and volume setting for different frequency ranges, we could only use one region in the frequency space at a time). We had to be careful, though, to replace the sensor at the origin after each run, since it didn't exactly go back there.

3.4.2 Q-factor

Using the program `drumsamp`, we could record the amplitude of oscillation of the plate in function of time (using the Lock-In signal for the amplitude, as usual, and the computer clock to record the time). Immediately after having started the program, we turned off the speaker, so that we could record the damping behaviour of the plate. This will be used in the data analysis section to compute the Q-factor.

3.5 Complementary Measures

3.5.1 Hysteresis

To study the non-linearity of vibrations of the plate, we drove the fundamental mode with a loud enough volume so that we could start hearing the *plate* vibrating! We then measured the amplitude spectrum at the origin of the plate with the `drumscan` program, with one run going from lower to higher frequencies, and another run going from higher to lower frequencies (so that we could study hysteresis).

3.5.2 Perturbation and degeneracy

We finally tried to excite the simple modes of the 1-2 degenerate mode found at 217 Hz, by changing the direction of the speaker. More on this in section 4.4.

4 Results and Data Analysis

4.1 Determination of resonant frequencies and Mode Mapping

As explained in section 3.4.1, the program `drumscan` permitted us to scan the whole plate for an amplitude spectrum at each point. To analyze this data, we used the program `drumscan_process`, also programmed in C by Mark Orchard-Webb. This program could mainly do two things for us: it could output the amplitude spectrum at the point where the maximum amplitude of vibration occurred in the grid (and also gave at which frequency this maximum was recorded). It could also return a 3D surface plot with contour lines of the maximum amplitude at each of the grid point (maximum over all frequencies at each point). This latter option was used to identify which mode of vibration was excited, by comparing them with the theoretical modes which were obtained from equation (6) in section 2.1. The former option will be useful in the Q-factor part (see section 4.2). In the next section, we present a qualitative analysis of the mode shapes obtained.

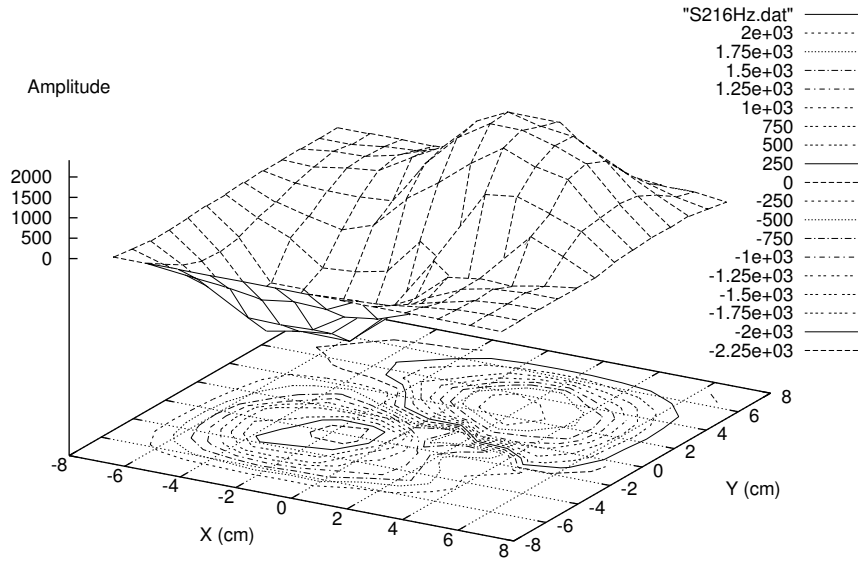

Figure 6: `Drumscan_process` **3D surface output representing the amplitude scanning for the 210Hz to 226Hz range.** This scan was taken using a 13x13 grid on a 14 by 14 cm square of the plate centered at origin. The maximum amplitude was recorded at the position (-1.2 cm, -2.3 cm) and at the frequency of 217 Hz. The number of amplitude measures taken by the computer for each specific frequency and grid point was 2048. The number of frequency steps taken in the 210Hz to 226Hz was 240. The scanning took about 8 hours.

4.1.1 Mode Mapping

The 3D plotting option of the `drumscan_process` program was useful to provide a quick way to visualize the data. An example of the 3D plot it produced for the amplitude scanning in the 210 Hz to 226 Hz region is shown in figure 6. 3D plots depicting the theoretical shapes for the first modes of vibration (simple and degenerate up to the 5-5 modes) of the plate were provided to us by Mark Orchard-Webb. The 1-2 degenerate mode is shown in figure 7. We can easily see that this theoretical mode is very similar to the one we obtained in the 210 Hz to 226 Hz region.

We considered the resonant frequency to be the frequency at which we obtained the maximum amplitude of vibration (this was outputted by the analysis program). By looking at the shape of the amplitude spectrum at the point of highest amplitude in the grid (also given by the analysis program), we could see

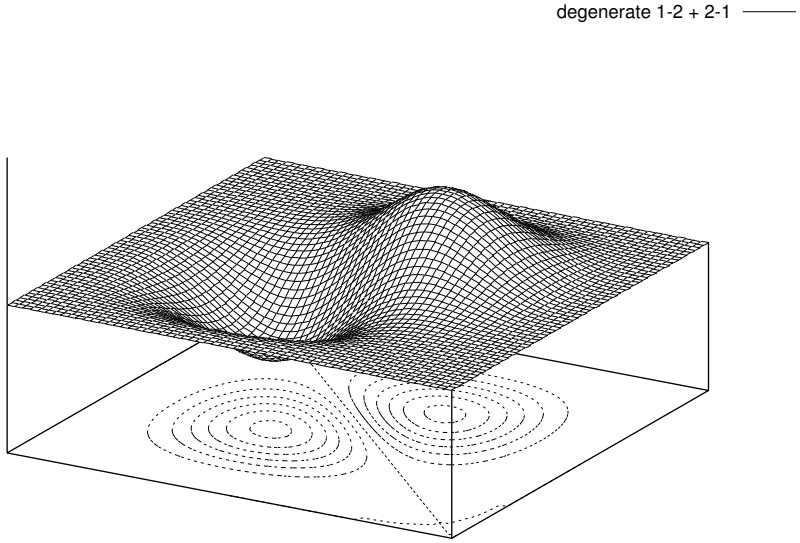

Figure 7: **Theoretical shape of the 1-2 degenerate mode.** This picture was provided to us by Mark Orchard-Webb.

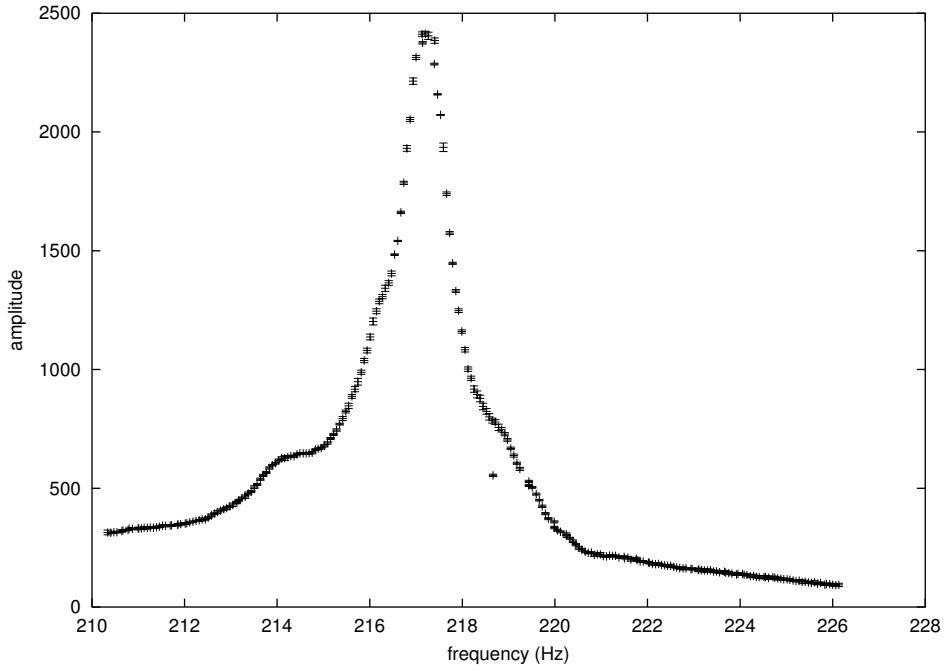

Figure 8: `Drumscan_process` **max amplitude spectrum output for the amplitude scanning in the 210Hz to 226Hz range.** This data is associated with the one used in figure 6. This graphs the average amplitude recorded at the point (-1.2 cm, -2.3 cm) of the grid (where the global maximum of amplitude was recorded) for each frequency (2048 measures per frequency). The error bars on the graph come from the standard deviation computed by the `drumscan` program while taking the 2048 measures.

it was justified. An example for the 210 Hz to 226 Hz range is shown in figure 8. The maximum amplitude was recorded at 217 Hz. We could guess at first sight of this graph that the main peak represents a Lorentzian (as is predicted by the theory for harmonic oscillator in section 3.4.2 in equation (15) and figure 1). And indeed the 217 Hz peak is in the middle of this Lorentzian. The Lorentzian shape will be discussed more in section 4.2 about the Q-factor.

We have mapped the vibration modes for the first 4 resonant frequencies of 103, 217, 342 and 408 Hz, as well as for the 684 Hz frequency. Those frequencies correspond to the frequency where the maximum amplitude was reached. The mode shapes obtained are presented in appendix B, with the theoretical graphs for comparison. The mode mapping is summarized in table 2, in next section. As a whole, we can say that we have a very good correspondence between our measured mode shapes and the theoretical ones. For comparison (and to witness that there is no doubt about our matching), the other first theoretical modes

are also given in appendix B. Note that for each mode where there could be degeneracy (the 1-2 and 1-3 modes in our case), we have obtained the degenerate mode rather than a specific simple one. This makes sense since physically, if our system is symmetric, there shouldn't be any reason why one of the simple modes should be more excited than the other. So we obtain an equal linear combination of the two (the degenerate mode). This means that our system was indeed approximatively symmetric.

It should be mentioned that the `drumscan_process` program uses the maximum amplitude found at a specific point *for all frequencies*, to produce those 3D plots. But since the amplitude of vibration is so much greater at a resonant frequency than at other frequencies, we can assume that the graph produced by `drumscan_process` represents well the shape of the vibration of the plate *at the resonant frequency*. When we compare the result in figure 6 with the theoretical mode in figure 7, we can conclude that this is a justified assumption. On the other hand, an option in the `drumscan_process` program permitted us to isolate certain frequency ranges, so that if we had two resonant frequencies in the same datafile, we could graph the amplitude plot of each one separately. This gave us the occasion to study the difference between the simple 1-3 mode and the degenerate 1-3 mode, as will be described now.

Figure 9 shows the amplitude spectrum for the 375 Hz to 427 Hz range. This was used to study the mode shape of the 408 Hz resonant frequency. A very noticeable second amplitude peak can be seen on this graph around 396 Hz. For this range of frequencies, the mode shape found was identified to be the 1-3 degenerate mode. But guided by the strange peak at 396 Hz, we decided to investigate (isolate) the mode shape for frequencies under 398 Hz (where it was noticed on the graph that the amplitude peak at 396 Hz became dominant). It appeared that this mode shape was the *simple* 1-3 mode! For a better visualization tool, we used Matlab. The comparison between the 375 to 427 Hz range mode shape with the 1-3 degenerate theoretical mode is shown in figure 10. The isolated mode shape for the 375 to 398 Hz range is shown in figure 11, with the theoretical 1-3 simple mode.

This split could be due to small perturbations on the plate which would be frequency dependant. Drawing a parallel to quantum mechanics and the perturbation theory, the degenerate mode 1-3 can split in two different eigenfrequencies when a small perturbation is included. The fact that we still obtained the 1-3 degenerate mode (instead of obtaining the 1-3 and 3-1 modes with different frequencies) suggests us that this perturbation could depend on the frequency (so that it doesn't affect the plate at 408 Hz, for example). This kind of perturbation could be induced by vibration modes of the drum assembly frame, for example.

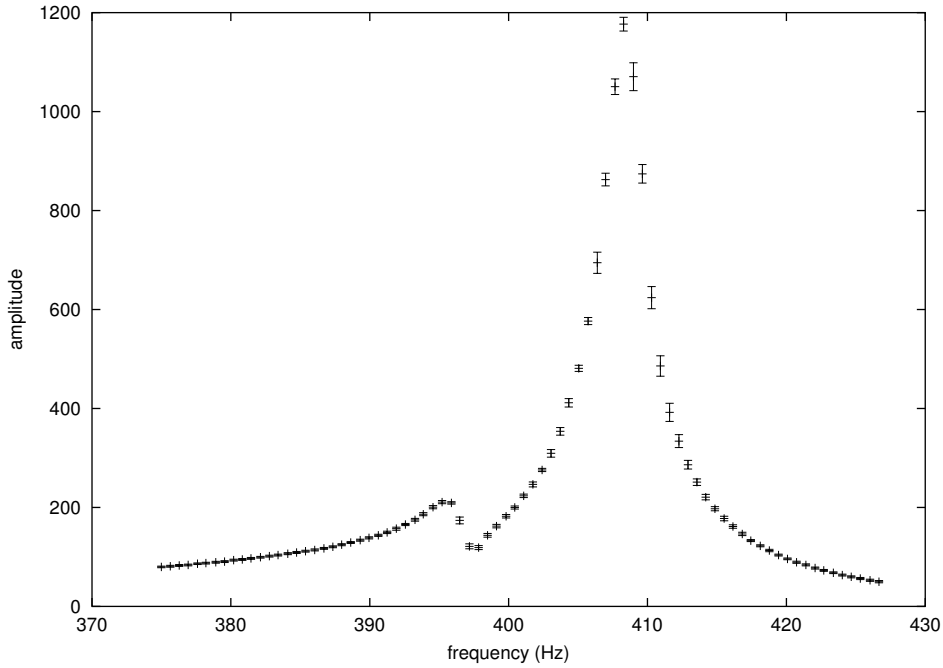

Figure 9: **Amplitude spectrum for the 375 Hz to 427 Hz range.** The resonant frequency was found to be at 408 Hz. Notice the second peak of amplitude at 396 Hz.

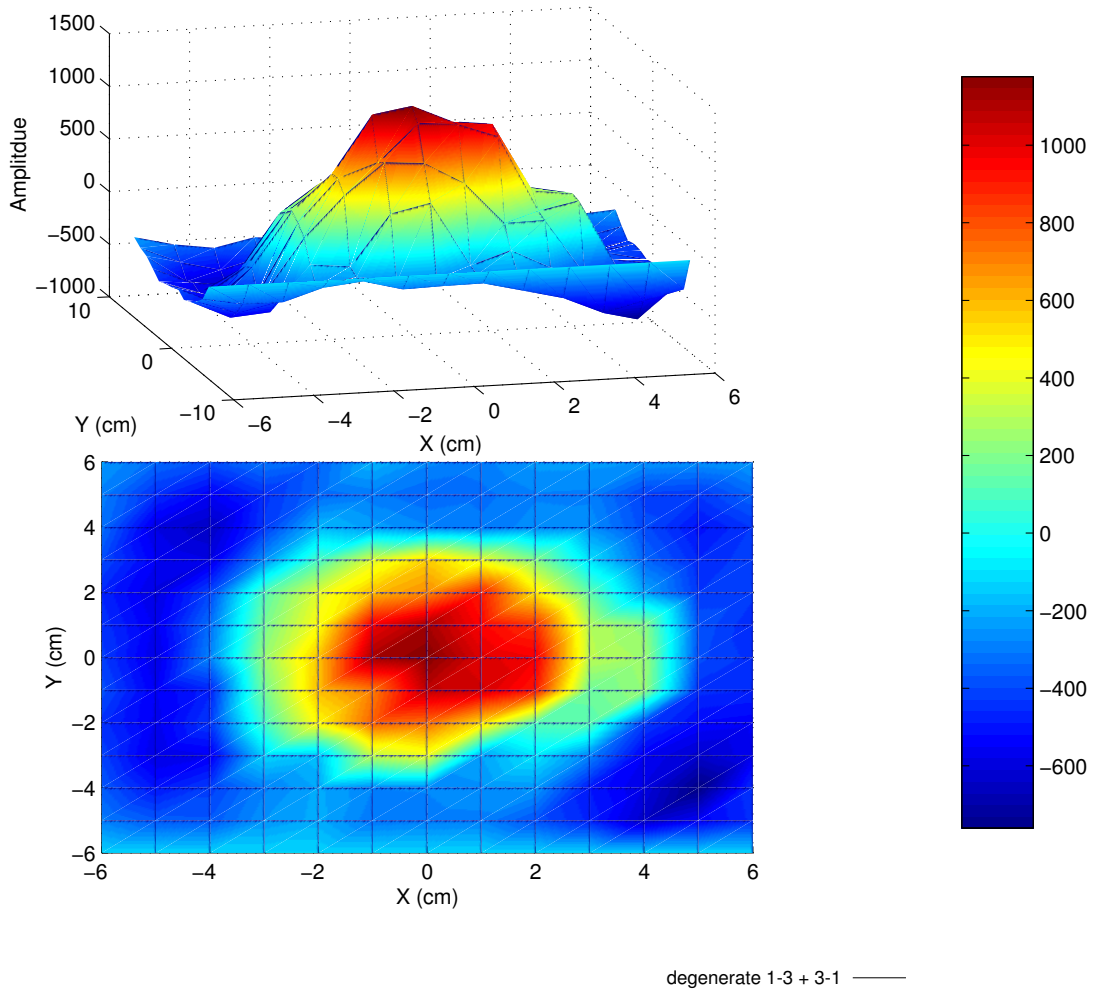

Figure 10: **Mode shape for the 375 to 427 Hz range.** The 1-3 degenerate theoretical mode is depicted at bottom.

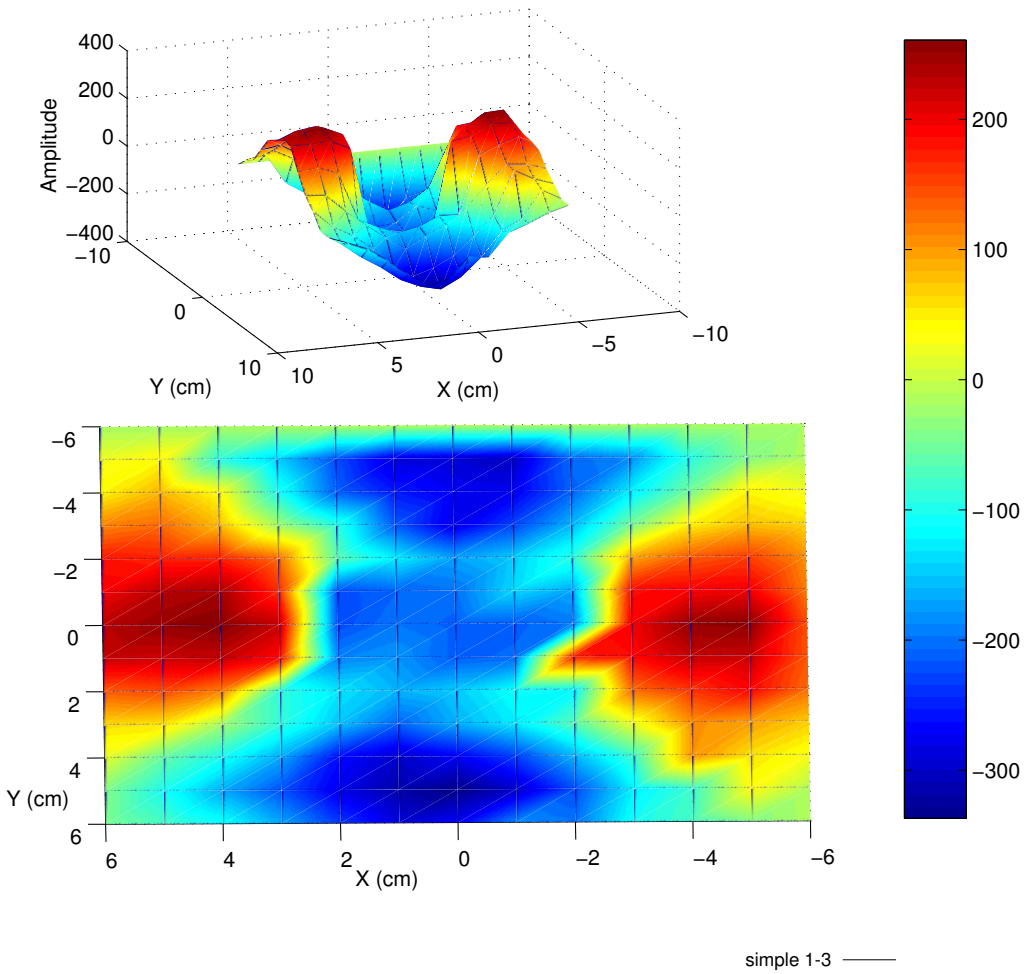

Figure 11: **Isolated mode shape for the 375 to 398 Hz range.** The 1-3 simple theoretical mode is depicted at bottom.

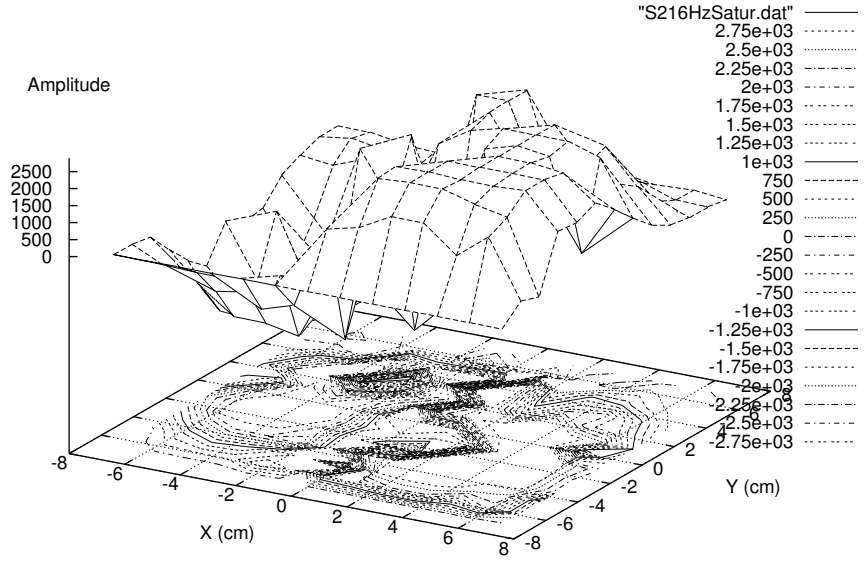

Figure 12: **Example of saturation.** This represents a mode shape taken in the frequency region around 217 Hz when the ADC input was saturated.

Finally, we give an example of saturation of the ADC input. A mode shape for the frequency region around 217 Hz when the Lock-In was badly calibrated is shown in figure 12. We can see that it is not clear if this represents a 1-2 simple or degenerate mode. This reminds us of the importance of good calibration; but it was in fact very hard during this experiment to obtain the proper settings on the first shot.

4.1.2 Resonant frequencies

We recall equation (7) which gives the eigenfrequencies of vibration of the plate:

$$f_{ij} = \frac{{\lambda_{ij}}^2}{2\pi a^2}\sqrt{\frac{D}{\rho}} \equiv A\,\lambda_{ij}^2 \tag{19}$$

where A becomes a constant characteristic of the plate, and the λ_{ij}'s depend on the mode of vibration and are given in [6]. This equation gives a linear relationship between the resonant frequencies f_{ij} and the dimensionless λ_{ij}^2 which we can use to find the constant A using our measured frequencies. Table 1 gives the values of the physical parameters characterizing the plate and which gives

Length	a	$(1.50 \pm 0.01) \times 10^{-1}\ m$
Thickness	h	$(3.1 \pm 0.1) \times 10^{-4}\ m$
Density of aluminum		$2.77 \times 10^{3}\ kg/m^3$
Young's Modulus	E	$7.24 \times 10^{9}\ N/m^2$
Poisson's Ratio	ν	0.33
Mass/unit area of plate	ρ	$0.86 \pm 0.06\ kg/m^2$
Flexural Rigidity	D	$0.20 \pm 0.02\ N \cdot m$
proportionality constant	A	$3.4 \pm 0.2\ Hz$

Table 1: **Parameters for our setting** The second part of the table gives computed values.

Mode	λ_{ij}^2	measured freq ± 5 Hz	theoretical freq Hz
1x1	36.13	103	123
1x2	73.75	217	251
2x2	108.80	342	370
1x3	132.50	408	450
2x3?	165.88	522	564
3x3	220.90	684	751

Table 2: **Measured frequencies of resonance and mode mapping.** We note that we haven't done the mode shape scanning at the 522 Hz frequency, so that's why we put an interrogation mark beside the 2x3 mode. The 5 Hz error was estimated by the shift in resonant frequencies that we regularly observed (due to temperature changes, for example).

a value for A. Note that the relatively big incertitude on A is caused mainly by the big incertitude on the thickness of the plate.

Table 2 gives the resonant frequencies that we have measured (using the maximum amplitude during the mode scan; except for the 522 Hz frequency which was simply measured using the oscilloscope), together with the theoretical frequencies predicted using the *measured* A according to equation (19). Those results are also depicted in a graph in figure 13, where a linear fit is done through our measured frequencies of resonance in function of λ_{ij}^2. The value of A obtained is 3.2 ± 0.1 Hz; which is just inside the range of the the 3.4 ± 0.2 value predicted by the theory. But most importantly, we truly see on this graph that the relationship between f_{ij} and λ_{ij} is linear. We can also observe on the graph that all our measured resonant frequencies are lower than the theoretical predictions. This could be due because air resistance was neglected when deriving the equations of motion of the plate in section 2.1. But air truly plays an important role in this system since it is responsible for the driving of the plate. Moreover, according to the theory of simple harmonic oscillators, we

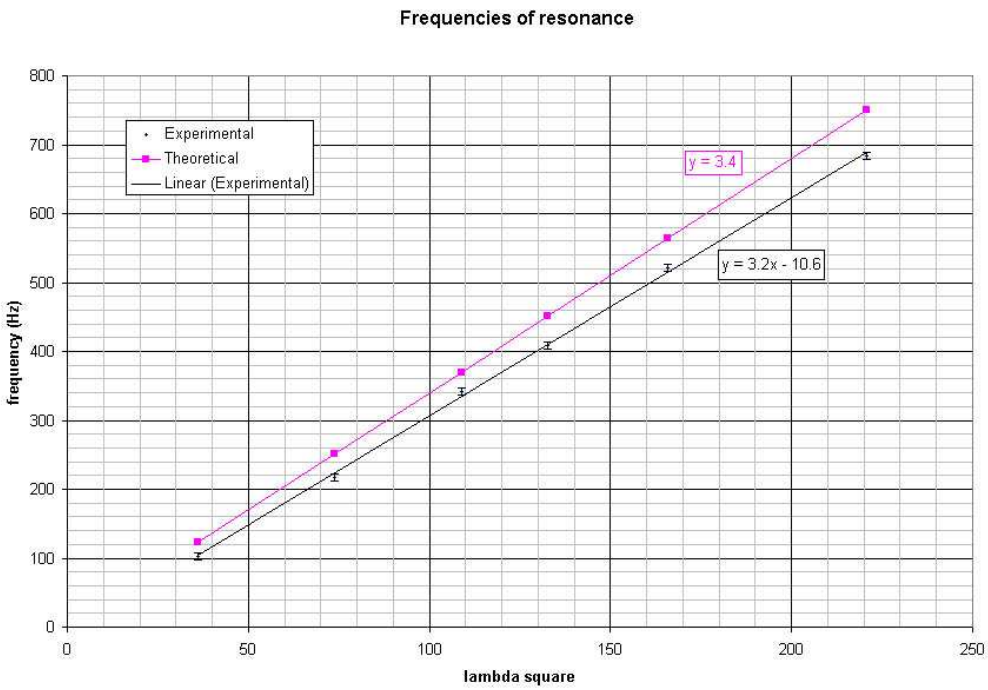

Figure 13: **Frequencies of resonance** The pink line is the theoretical prediction for frequencies of resonance according to the parameters of our plate. The black line is a linear fit through our experimental data.

frequency Hz	γ Hz	Q-factor (decay)	Q-factor (width)
103	17.2 ± 0.4	38 ± 1	88 ± 20
408	16.6 ± 0.4	154 ± 4	146 ± 20

Table 3: **Q-Factor comparison between the decay method and the width method.** Both γ and Q-factor (width) were obtained using nonlinear fitting. The error on γ was given by the `nlparci` function in Matlab. The error on Q-factor (width) was estimated by changing the modelling equation (using simple or double Lorentzian; with fixed or variable resonant frequency, etc.) and observing the change in the resulting Q-factor.

know that the damping causes a shift of the resonant frequencies toward the lower frequencies, explaining our observation.

4.2 Q-factor

Using the program `drumsamp`[3], we obtained the sensor output in function of time just after we had shut off the speaker in order to observe the damping behaviour of the system. By subtracting the DC component of this signal and the resulting AC voltage, we obtained a quantity proportional to the square of the amplitude of vibration of the plate, and so proportional to its energy. We have measured this transient behaviour at the origin of the plate at 103 Hz and at 408 Hz (since they were the two only modes with a prominent maximum at the origin). We measured the signal for 1 second at a frequency of 1000 Hz. The resulting analyzed graph for the 408 Hz resonant frequency is shown in figure 14. Very similar results were obtained for 103 Hz. From equation (11), we see that we should obtain a decaying exponential. By fitting $E_0 e^{-\gamma t}$ with E_0 and γ as variable parameters, using the nonlinear fitting function `nlinfit` of Matlab, we have obtained an estimation for γ, and thus Q since $Q = w_0/\gamma$ according to equation (12) (with w_0 in rad/sec). The results for both frequency of resonance are given in table 3. We can see that the γ factor is the same (taking in consideration its error) for both frequencies, meaning that the damping is not dependent on frequency. This is what is usually assumed when considering a simple harmonic oscillator.

The other mean by which we could evaluate the Q-factor was with the FWHM of the energy peak in the frequency space. Figure 15 shows energy spectra for the 103 Hz and 408 Hz scans (obtained by squaring the amplitude

[3]To use this program, we needed to connect directly the sensor output to the Lab Master (without passing through the Lock-In amplifier). We thus needed to decrease the DC power source of the sensor to 12 V in order to obtain a voltage acceptable to the Lab Master. A quick calibration of the sensor showed that we stayed in the middle of the linear region of its response.

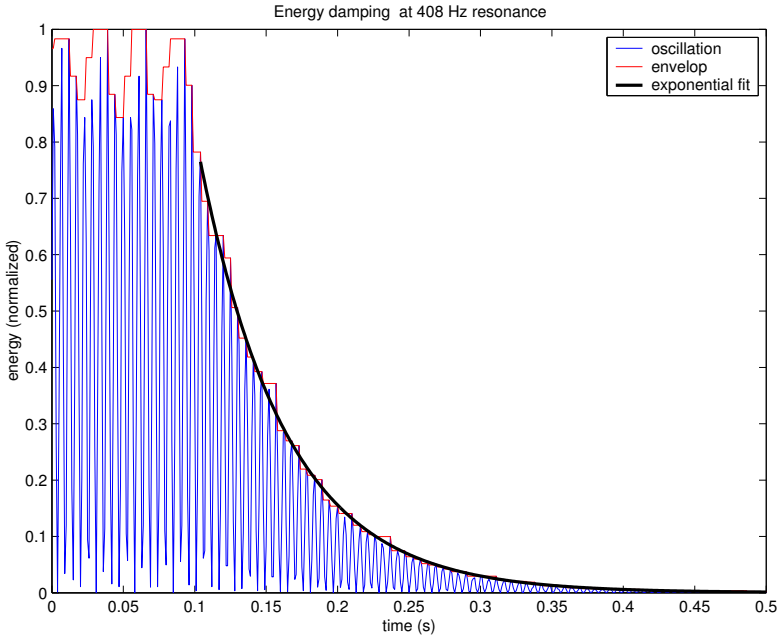

Figure 14: **Energy damping at 408 Hz resonance.** This represents the transient energy of vibration just after the speaker is shut off. The black line is from an exponential fit using Matlab.

spectrum). We present the double Lorentzian:

$$\frac{A}{\left(\frac{\omega}{\omega_0}-1\right)^2+\frac{1}{4Q^2}}+\frac{B}{\left(\frac{\omega}{\omega_1}-1\right)^2+\frac{1}{4Q_2^2}} \tag{20}$$

where all letters are variable parameters except w which is the independant variable. w_0 and Q are the relevant resonant frequency and Q-factor respectively. We have fit this function in our energy spectra using Moosefit. The Lorentzian shape was suggested according to equation (15), and the addition of two Lorentzians was suggested by the dedoubling of the resonant frequency, as already discussed in figure 9, in section 4.1.1. The result has been that the energy curve does seem similar to a Lorentzian (as we can see in figure 15), but it was really hard to make converging the fitting algorithm (we have proceeded by steps; starting with the resonant frequencies constant and then letting them vary) (explaining the big error estimate we gave on Q). Q was a parameter in the fitting function, so the fitting program gave it directly. But it should be equivalent to setting γ to be the FWHM of the peak.

We give the resulting values of Q using the Lorentzian model also in table 3. We see in this table that the Q-factors for the two different means of computation agree for 408 Hz but differ significantly for 103 Hz. This isn't too much alarming, since we noticed that the amplitude spectra were varying a lot from one run to another, and sometimes had weird shape as in figure 8. We consider the Q-value derived from the exponential decay method to be more trustful since it yielded more coherent results from one run to another, and also because it assumes less about the behaviour of the oscillating system (vs. considering the energy spectrum to be a Lorentzian). But what is qualitatively important is that they have the same order of magnitude, and that we can conclude that the vibrating plate is lightly damped.

4.3 Non-Linearity

Two graphs are shown on figure 16 comparing the amplitude spectrum obtained when increasing the frequency vs. when lowering the frequency, for two different volume levels. This amounts to follow different paths in frequency space. Both graph were taken at the origin of the plate, for the fundamental mode; and 200 measures were taken per frequency steps. The top graph corresponds to a loud driving, but not enough to make the plate emitting a distinctive vibrating sound. We see on this graph that the response is non-linear (since the curve is not symmetric), but we don't see any hysteresis yet since both paths yield the same response. On the other hand, the lower graph of figure 16 corresponds to a sound level where we just started to hear the plate vibrating. We clearly see on this graph that the amplitude spectrum depends whether we are going from left to right or right to left in the frequency space, and thus undergoes hysteresis. We can compare figure 16 with figure 3 in section 2.4 to clearly see a correspondence with classical nonlinearity theory. Surprisingly, though, there was a sharp transition between when there was hysteresis and when there

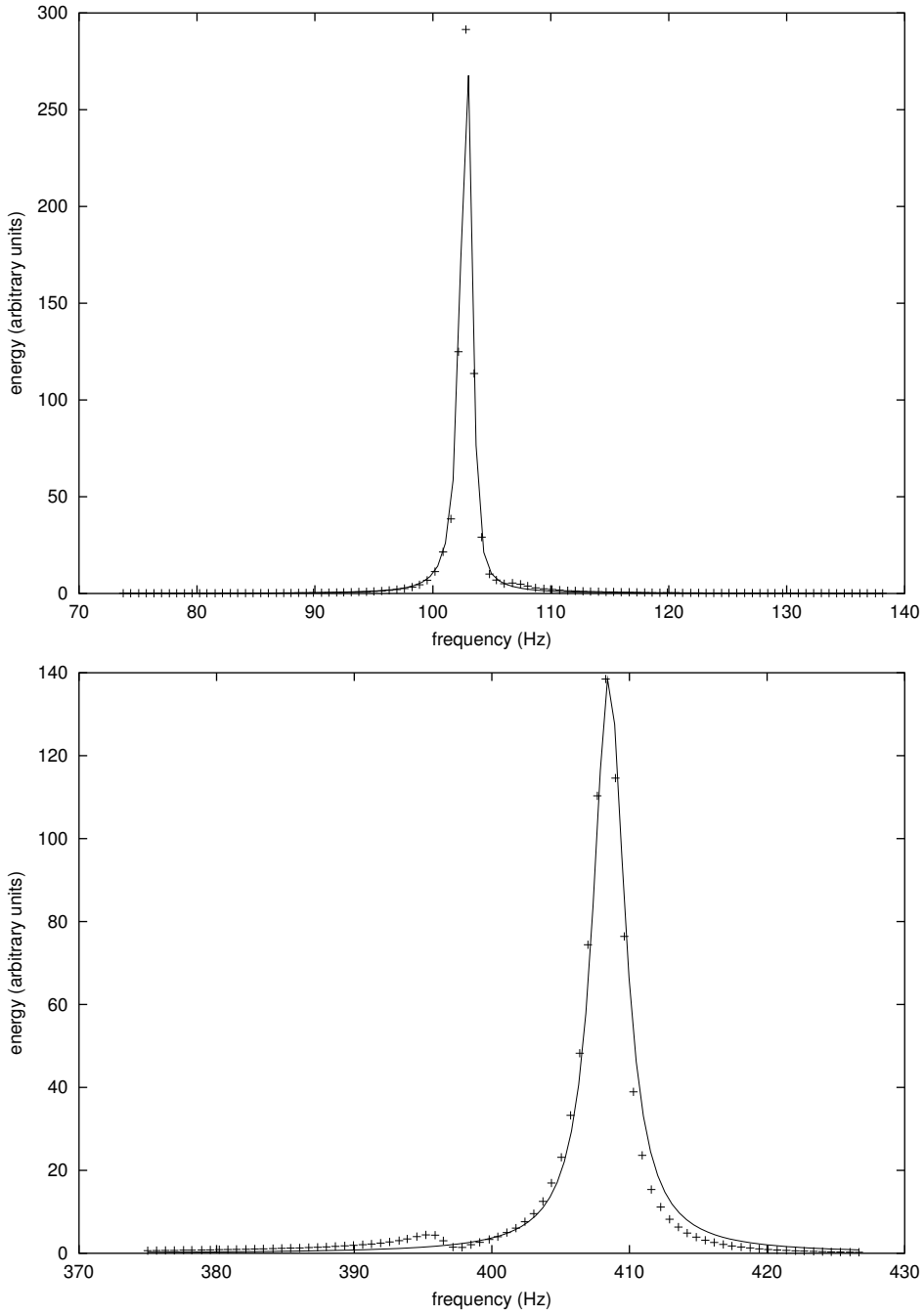

Figure 15: **Lorentzian fitting in the energy spectrum. Top: 103 Hz spectrum. Bottom: 408 Hz spectrum.** The curve drawn is a double Lorentzian fit done with Moosefit (for both graphs). The energy units don't mean anything in particular here.

was none. By putting the volume just below the level where we would hear the plate vibrating, we see no hysteresis at all; and then, by putting it some epsilons above, we could witness a clear effect of hysteresis, as if the phase transition wasn't continuous. Maybe some power-law could be associated with this phase transition...

4.4 Perturbation of Degenerate Modes

On the last day of experimentation, we tried quickly to perturb the degenerate 1-2 mode obtained at a frequency of 217 Hz. Using a 7x7 grid and a 30 steps frequency range, we could scan the 217 Hz mode in half an hour with the speaker in different orientations and position. We did obtain simple modes of vibration instead of the degenerate one (because we had broken the symmetry of the system) (see figure 17), but the lack of resolution of the grid made the analysis very hard. We didn't succeed to obtain a precise correlation between the direction of the speaker and the direction of the mode we obtained (parallel to X or Y axis). But at least we have succeeded to break the degeneracy of the mode (as expected by perturbation theory).

5 Conclusion

The purpose of this experiment was the experimental study of an oscillatory system (a clamped vibrating plate) with the help of the computer. This system was simple enough to be understandable, but complex enough to possess interesting properties as degeneracy of modes or hysteresis. Lots of calibration and settings were needed to accomplish this task, giving us a good experience of experimental methods.

In a first step, we directly observed the natural frequencies of vibration, which are function of the geometry of the plate. Obvious correlations were exposed between the measured spectrum and the predicted values. On a qualitative basis, the mode shapes found gave an even stronger argument in favor with the theory. The Q-factor evaluation allowed us to conclude that our plate forms a lightly damped oscillator. It also explained the shift in the resonant frequencies we had measured. Attempts to remove degeneracies showed that it can be achieved by introducing an asymmetry in the system which advantages a particular mode. Finally, our observations proved the existence of the hysteresis in overdriven systems.

At once, we wonder if the setup used could allow further investigations in this domain. In hysteresis, the non-equilibrium state during the transition (from one amplitude to the other) lasts a few cycles and could be studied with the same tool used for the transient behaviour.

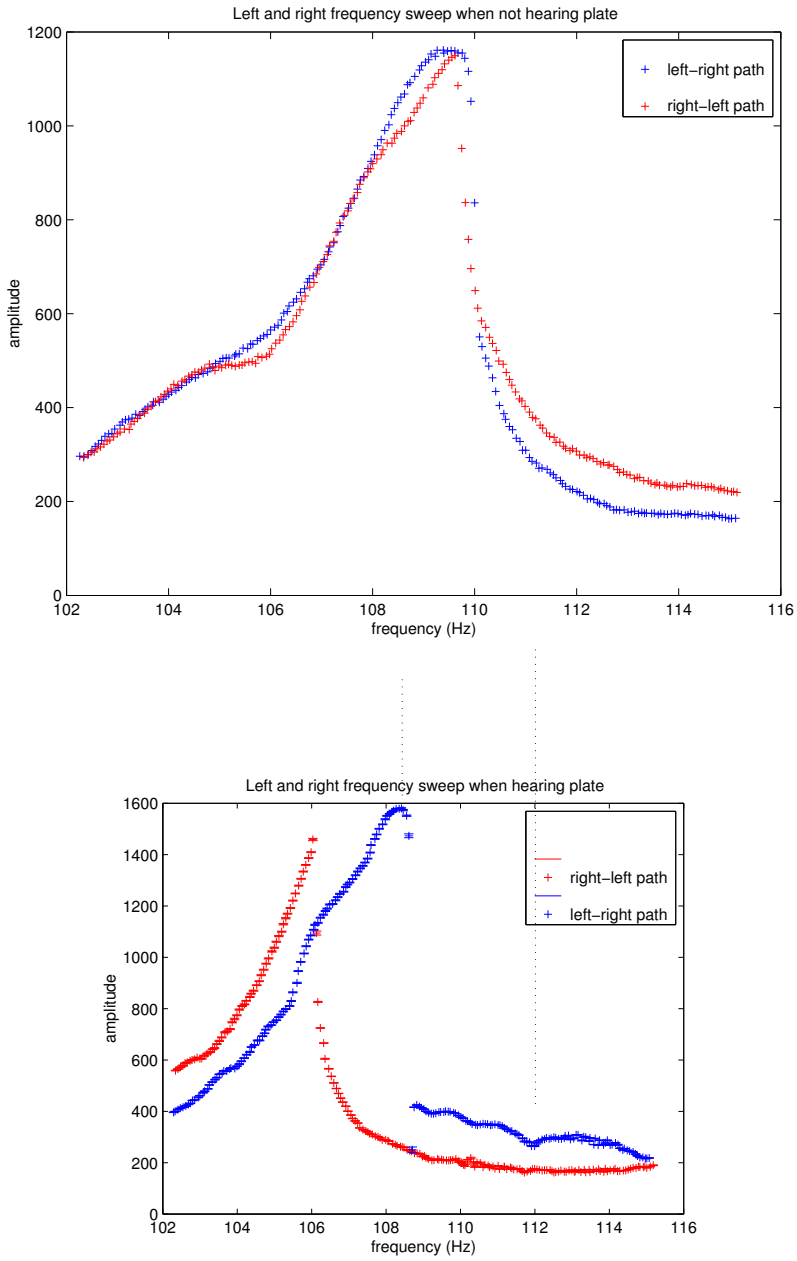

Figure 16: **Comparison between amplitude spectrum when increasing frequency vs. decreasing frequency.** The four curves were obtained at the origin of the plate. For the bottom graph, the plate was driven such that we could hear it vibrating; this wasn't the case for the top graph.

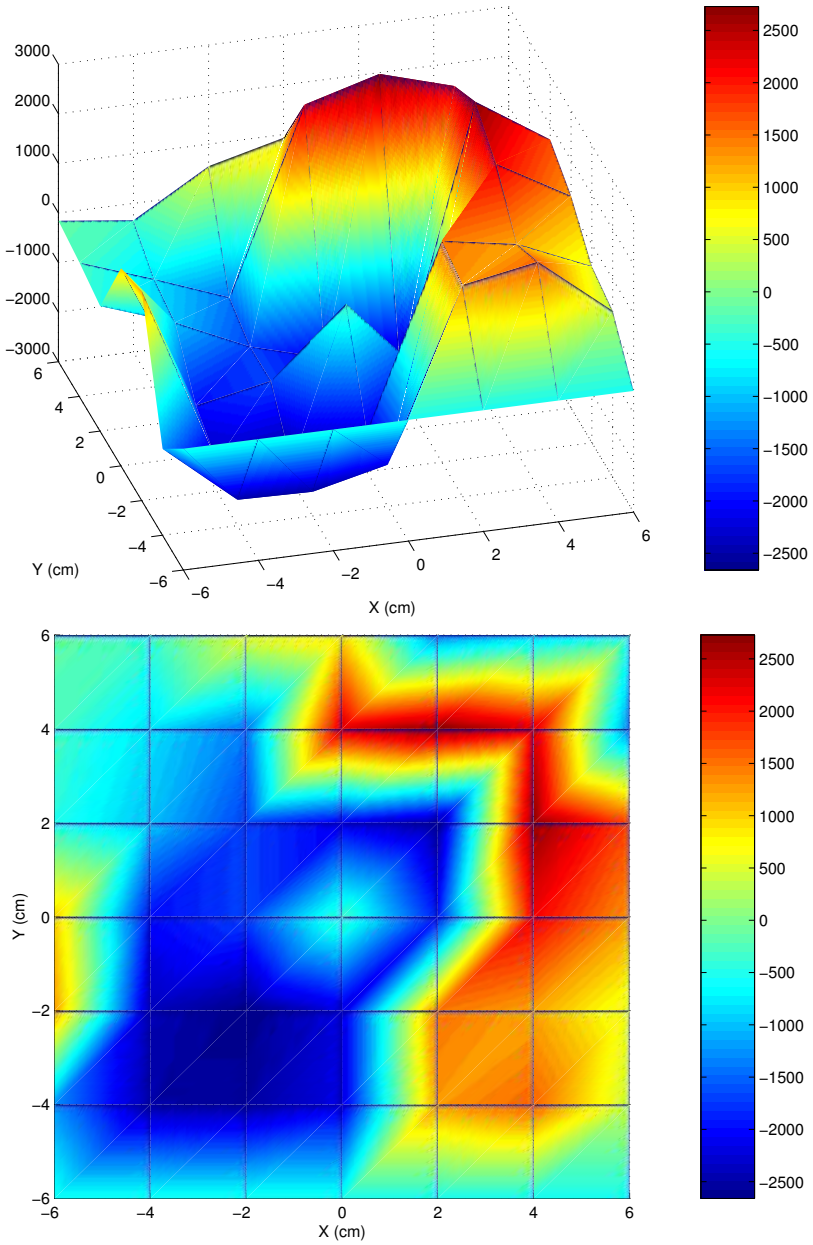

Figure 17: **Perturbation of the degenerate 1-2 mode (217 Hz).** This shape was obtained after having displaced the speaker to the left (of X axis). We clearly obtain a simple 1-2 mode.

6 Acknowledgments

We would like to thank Michel Beauchamp and Saverio Biunno for their constant technical support, Mark Sutton for his expertise in sensor's calibration, Fritz Buchinger for his constant help during the lab and Mark Orchard-Webb for the explanations about his programs.

A Calibration

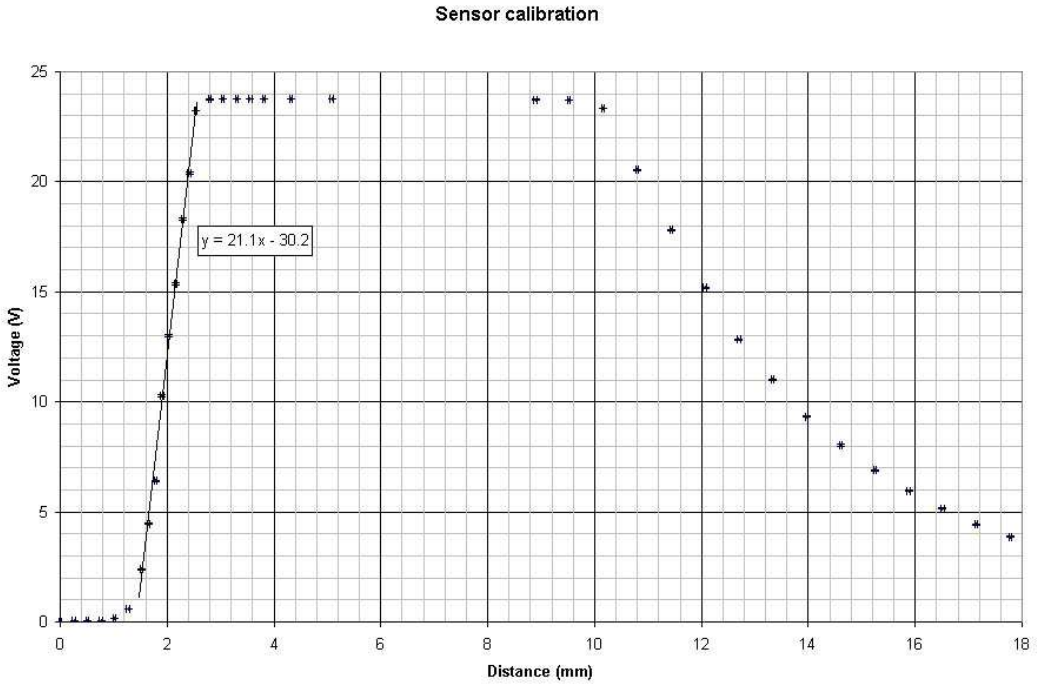

Figure 18: **Calibration curve for the sensor**

B Modes of Vibration

All the mode shapes that we have taken are presented in this annex, together with the corresponding theoretical modes, as provided by Mark Orchard-Webb. We have also included the other first theoretical modes as a reference. Those modes were obtained by using 13x13 grids, 15x15 grids or 20x20 grids, depending of when we ran them; and on 12 x 12 cm region or 14 x 14 cm region.

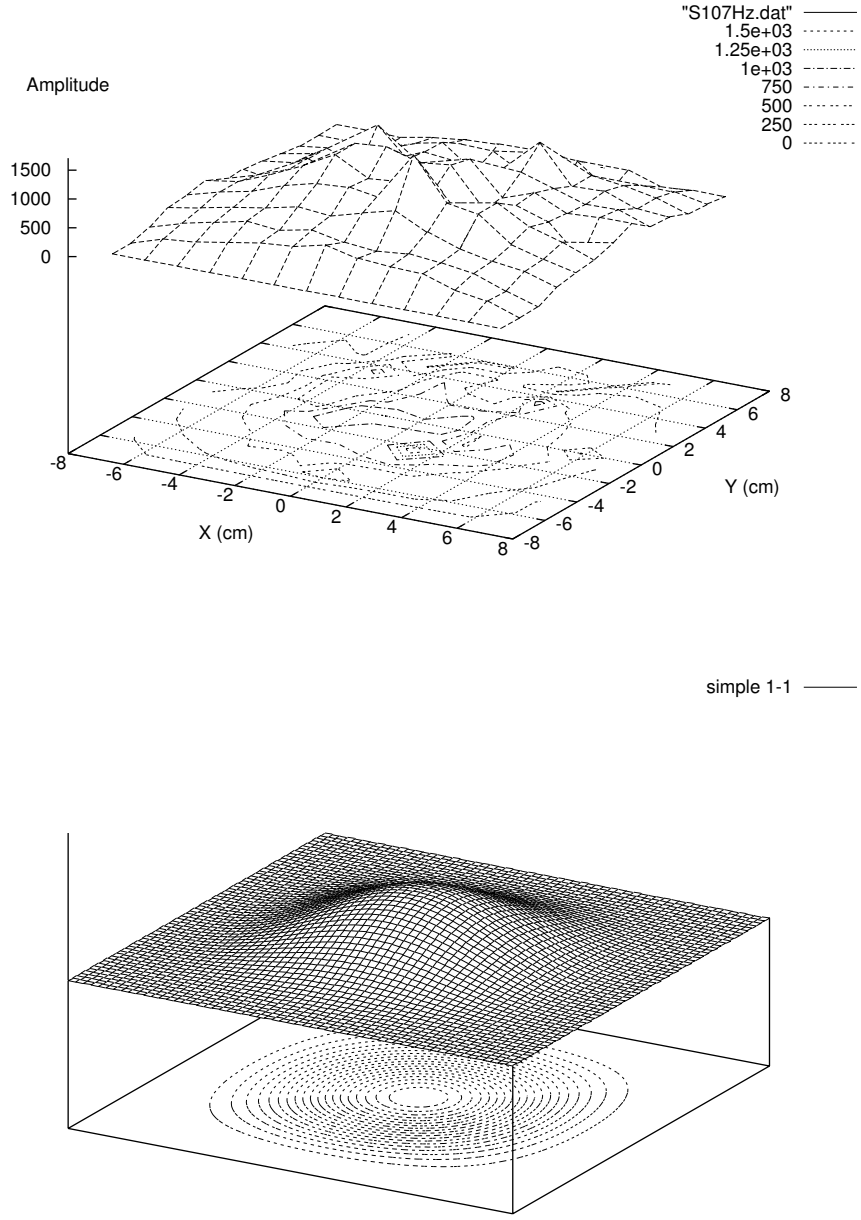

Figure 19: **Comparison between our amplitude map around 103 Hz and the simple 1-1 theoretical mode.**

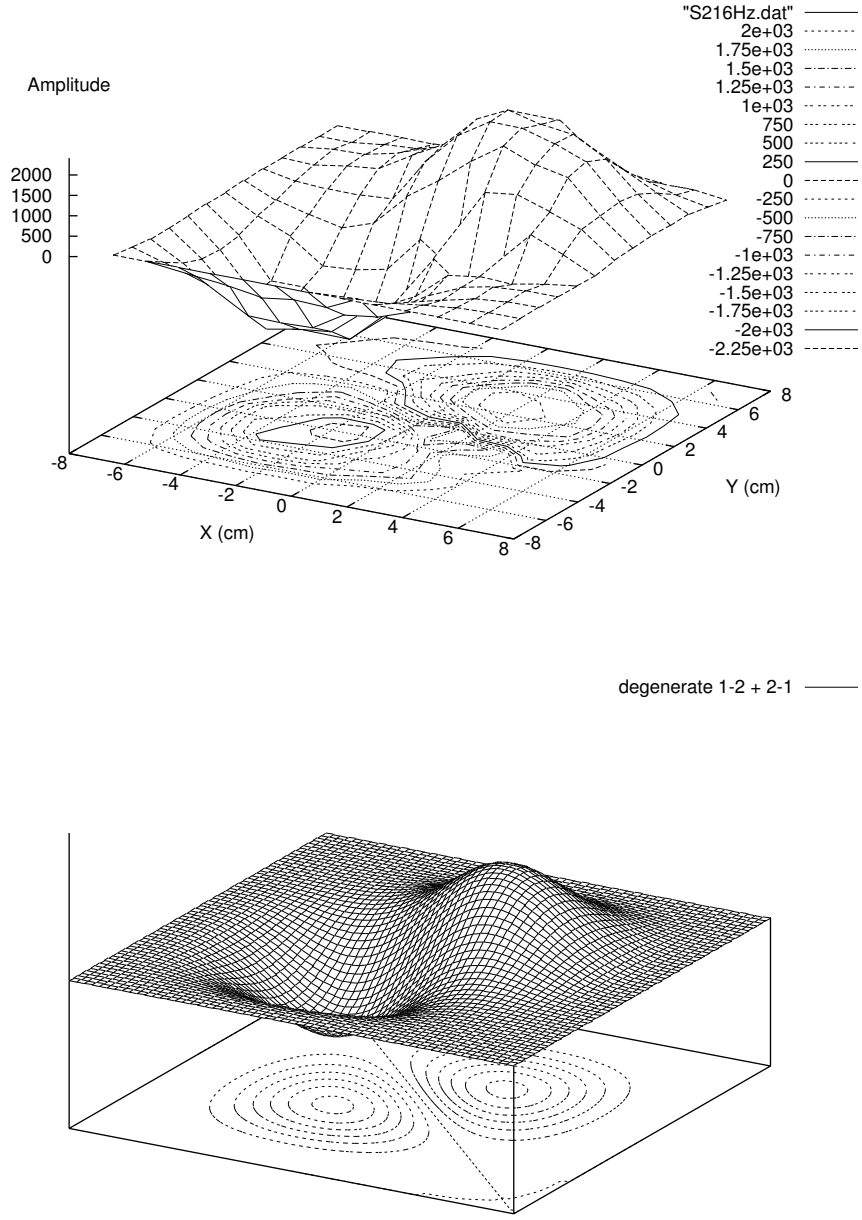

Figure 20: **Comparison between our amplitude map around 217 Hz and the degenerate 1-2 theoretical mode.**

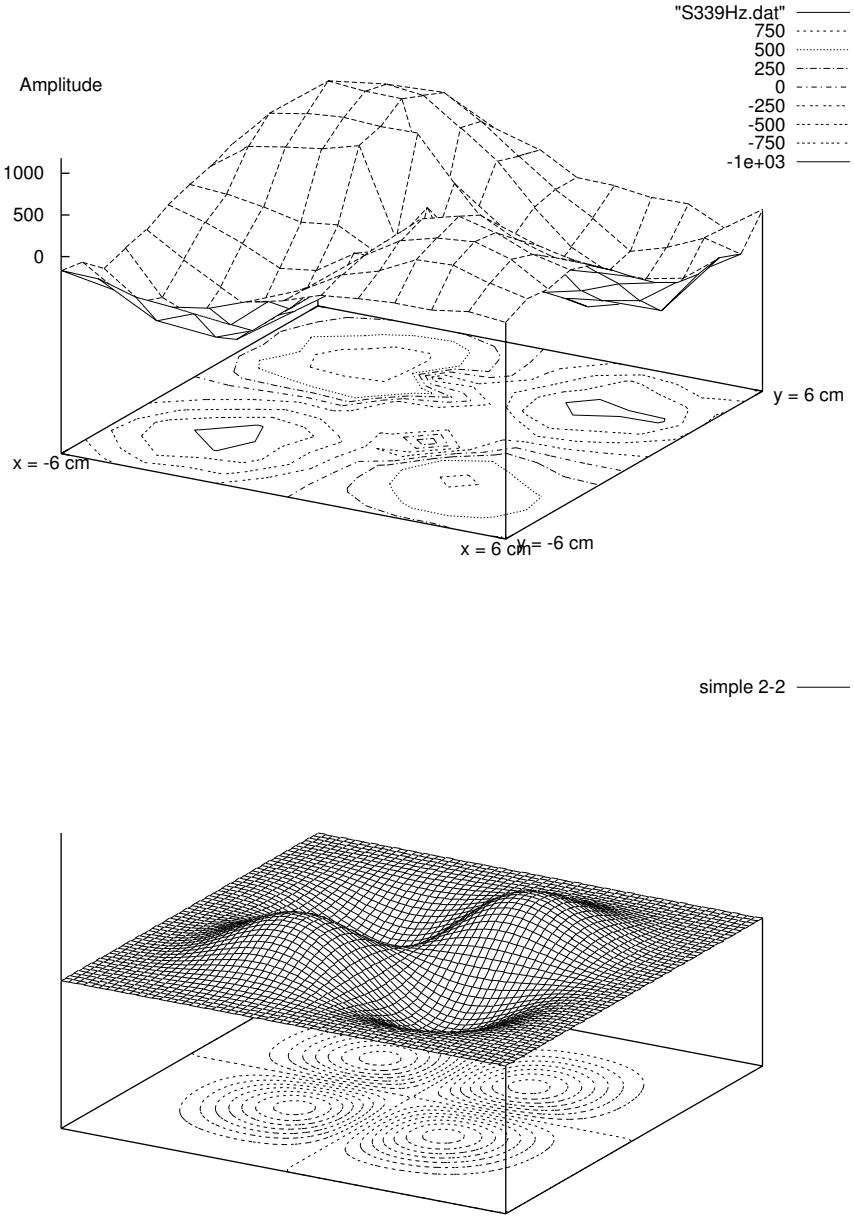

Figure 21: **Comparison between our amplitude map around 342 Hz and the simple 2-2 theoretical mode.**

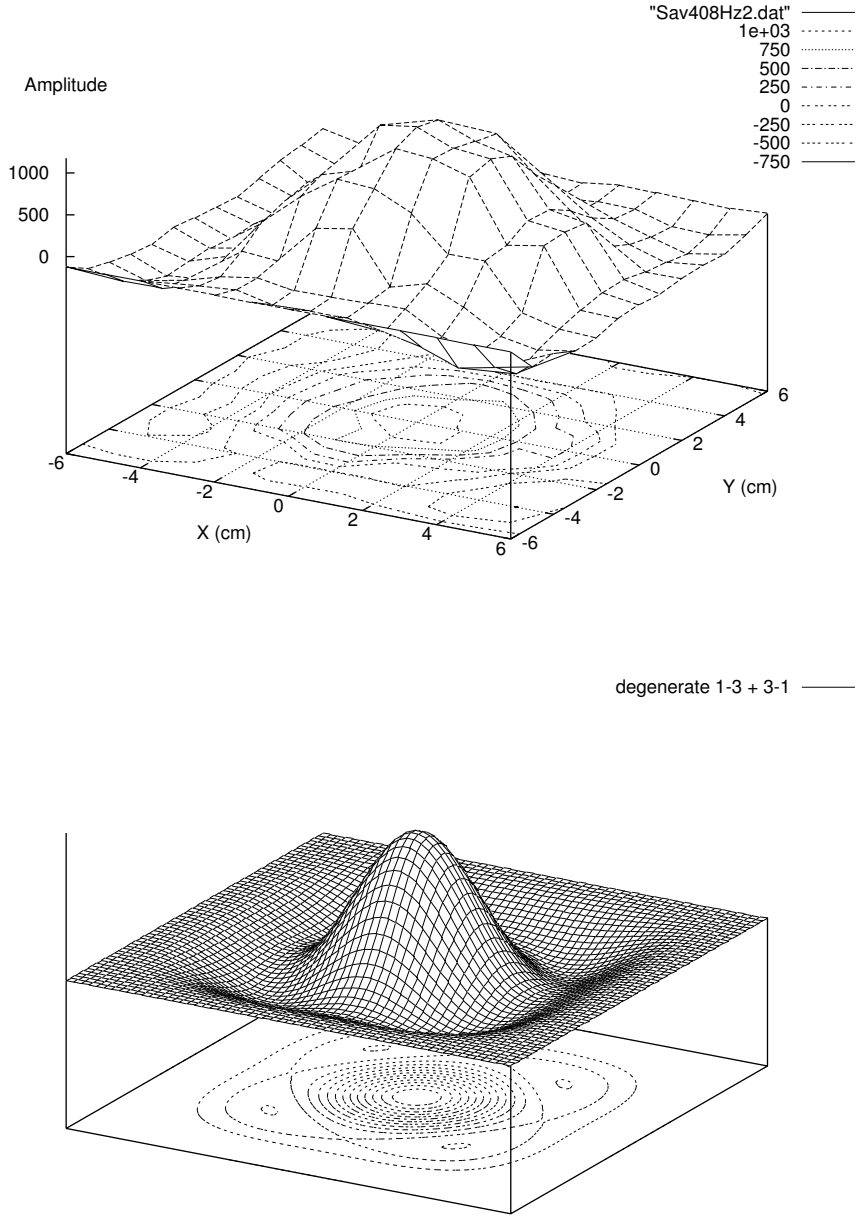

Figure 22: **Comparison between our amplitude map around 408 Hz and the degenerate 1-3 theoretical mode.**

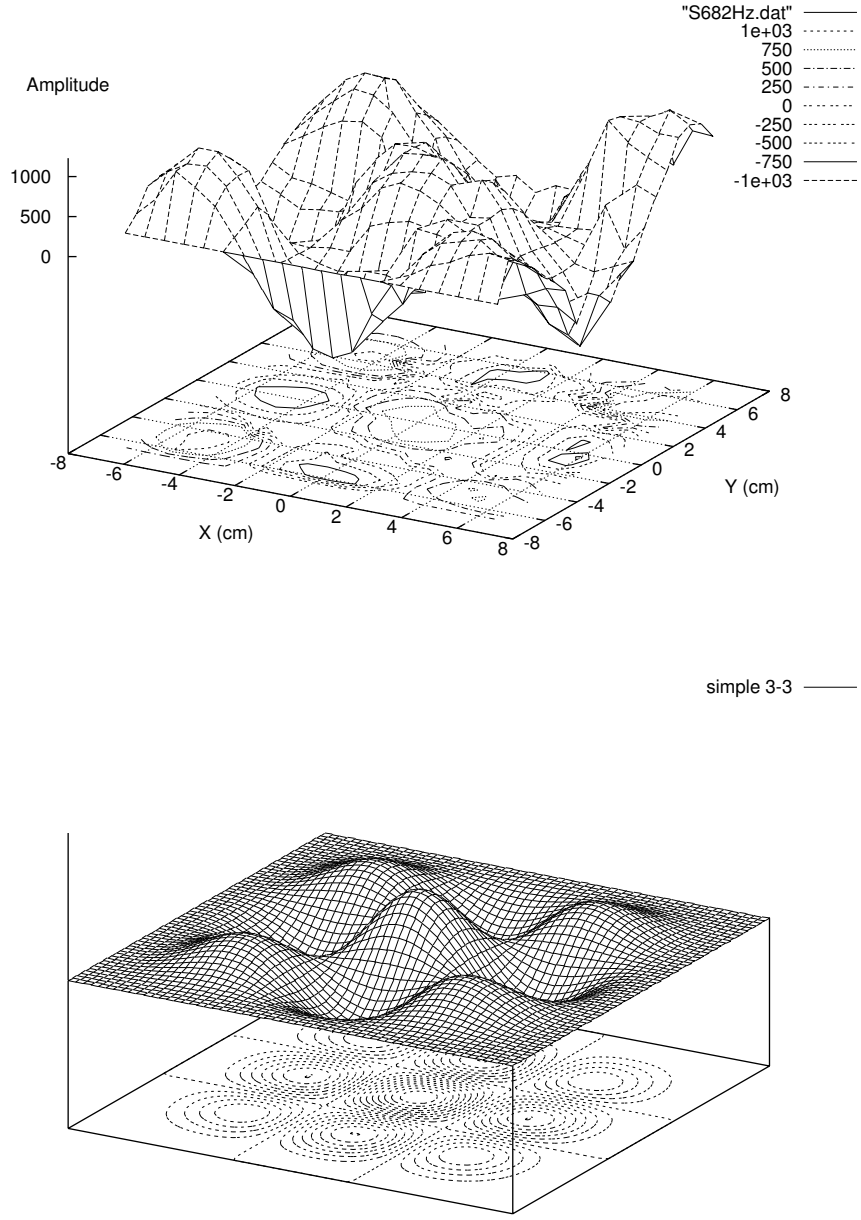

Figure 23: **Comparison between our amplitude map around 684Hz and the simple 3-3 theoretical mode.**

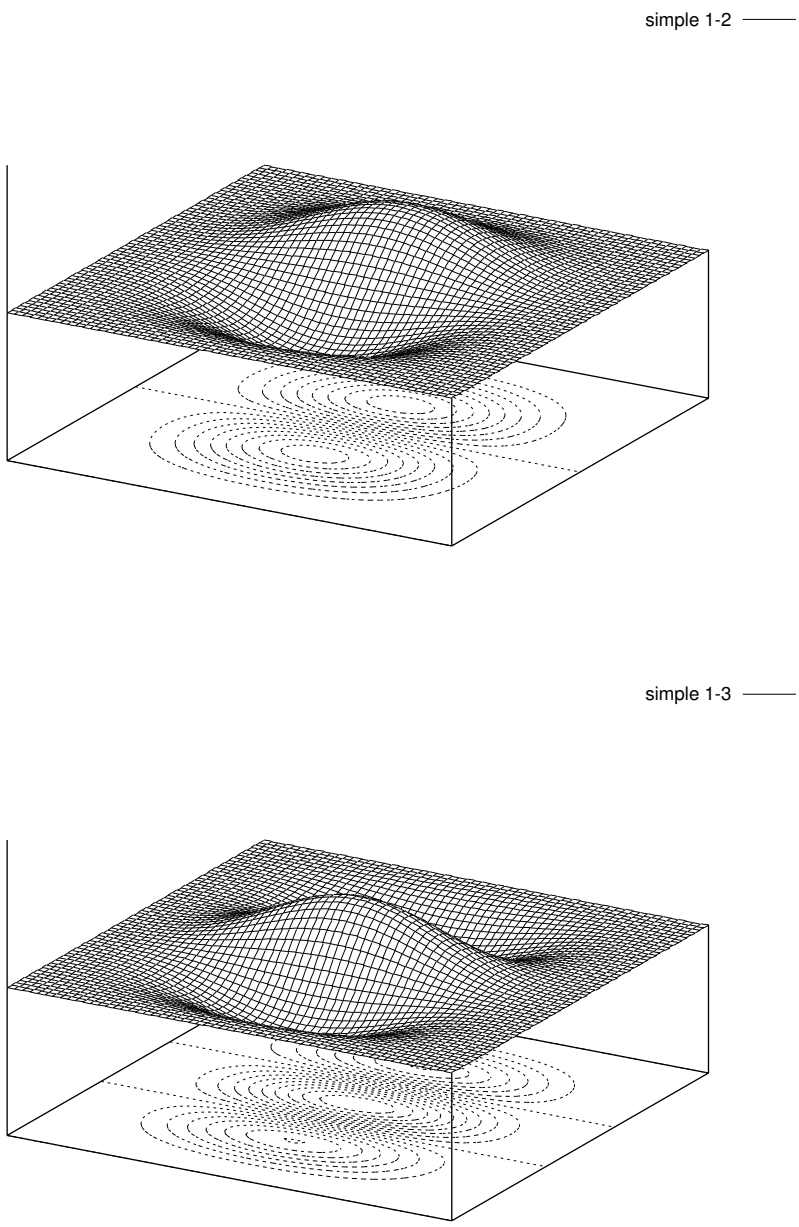

Figure 24: **Theoretical modes: simple 1-2 (top graph) and simple 1-3 (bottom graph).**

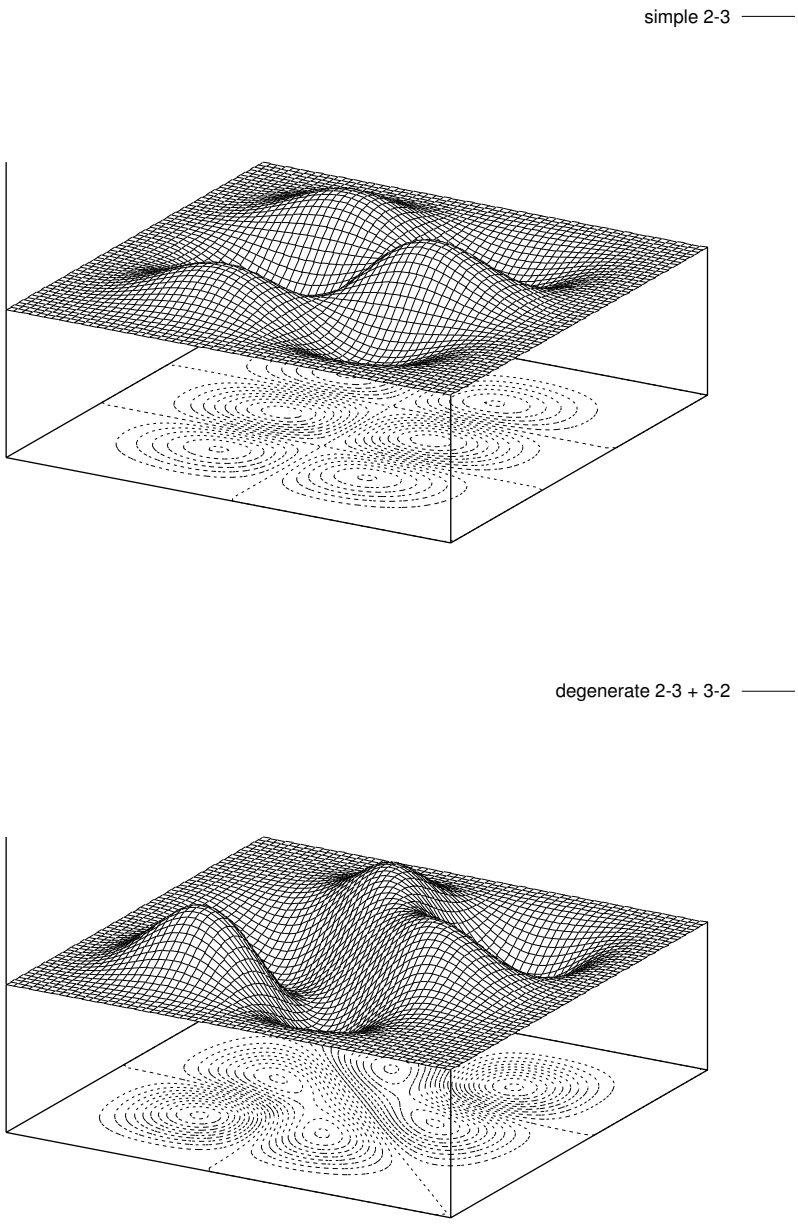

Figure 25: **Theoretical modes: simple 2-3 (top graph) and degenerate 2-3 (bottom graph).**

References

[1] Blevins, R.D., *Formulas for Natural Frequency and mode Shape*, Vas Nostrand Reinhold Co., New York, 1979
PSE: TA654 B54 2.1

[2] Harris, Cyril M., *Shock and Vibration Handbook*, 5^{th} edition, McGraw-Hill, New York, 2002 2.4

[3] Kleppner, Daniel and Kolenkow, Robert J., *An Introduction to Mechanics*, McGraw-Hill, England, 1960, pp.410-440 2.2, 2.2, 2

[4] Haberman, Richard, *Elementary Applied Partial Differential Equations*, 3^{rd} edition, Prentice Hall, Upper Saddle River, 1998
PSE: QA377 H27 2.1

[5] Landau, L.D. and Lifshitz, E.M., *Mechanics*, Pergamon Press, Oxford,, England, 1960, pp.84-93
PSE: QA805 L283 2.4, 3

[6] Leissa, A.W., *Vibration of plates*, NASA-SP-160, Office of Technology Utilisation, NASA, Washington D.C., 1969
PSE: TA660 P6L42 c.1 2.1, 2.1, 4.1.2

[7] Orchard-Webb, Mark and Kevin Di Filippo, *2-D Wave Phenomena For Dummies*, Department of Physics of McGill University, December 11 1998. 2.1, 5, 3.2.1, 3.2.6

[8] Nagle, R.Kent, *Fundamentals of Differential Equations and Boundary Value Problems*, 3^{rd} edition, Addison-Wesley, Reading, 2000
PSE: QA371 N243

[9] Reddy, J.N., *Theory and Analysis of Elastic Plates*, James Reed, Ann Harbor, 1998

[10] Timoshenko, S., *Theory of Plates and Shells*, 2^{nd} edition, McGraw-Hill, New York, 1959